Burrowing of nanoparticles on clean metal substrates: Surface smoothing on a nanoscale

C. G. Zimmermann,[1,2] K. Nordlund,[1,*] M. Yeadon,[1,†] J. M. Gibson,[1,‡] R. S. Averback,[1] U. Herr,[2,§] and K. Samwer[2,‖]

[1]*Materials Research Laboratory, University of Illinois, Urbana, Illinois 61801*
[2]*Institut für Physik, Universität Augsburg, D-86135 Augsburg, Germany*

We have investigated soft landings of Co nanoparticles on clean Cu(001) surfaces. The nanoparticles, ≈ 10 nm in size, were generated by dc magnetron sputtering in argon and transferred in the gas stream to an ultrahigh vacuum transmission electron microscope (TEM), where they were deposited on the thin-film substrate. The surface morphology created in this fashion exhibits a unique smoothing mechanism. The nanoparticles do not remain on the surface at temperatures as low as 600 K, but rather reorient and burrow into the substrate. By analyzing the TEM data in combination with molecular dynamics simulations, we were able to study this process in detail and to develop a model to quantify the temperature and cluster size dependence of burrowing.

I. INTRODUCTION

The smoothing of a rough surface was first addressed more than 40 years ago. Herring made a critical connection between surface morphology and surface chemical potential,[1] which Mullins later used to derive analytical equations describing the smoothing behavior of rough surfaces.[2] Recently the shrinking scale of microelectronic devices and the emergence of nanotechnology have provided renewed interest in the smoothing behavior of "artificially" created surface roughness on a nanometer length scale. While Mullins's description is in good agreement with experiments on the smoothing behavior of surface features produced by photolithography on Si,[3] the scale of roughness in these experiments is in the range of several thousand nanometers. Individual nanoparticles on single-crystalline substrates provide an ideal model system to study the smoothing behavior of roughness on a much finer length scale. In previous work the Mullins-Herring model of curvature-driven surface diffusion[4] appeared to explain the wetting behavior of nanoparticles for times sufficiently long compared to the initial particle substrate contact, where extremely high stresses are developed in the interface between the particle and the substrate.[5,6]

The purpose of this paper is to address the question of surface smoothing for the case where the surface energy of the particle is much larger than that of the substrate such that the particle does not wet the substrate. Recently we reported on the phenomenon of "burrowing" [7,8] of Co nanoparticles into Cu and Ag substrates. Burrowing provides the pathway for a system of metal nanoparticles on a single-crystalline substrate with lower surface energy to reach its quasiequilibrium configuration of many buried nanoparticles. This behavior is driven by capillary forces that force material to flow along the cluster-substrate interface. This mechanism allows the clusters to sink into the substrate. Here we report on the details of this novel surface smoothing mechanism, focusing on the system Co/Cu(001). A detailed analysis of the transmission electron microscope (TEM) data, in particular, a quantitative analysis of the strain contrast, in combination with molecular dynamics (MD) simulations, enables a deter-

mination of the depth of the particles and helps to elucidate their reorientation behavior. The details of the experimental setup and computer simulation model are summarized in Sec. II, while the experimental and computational results are presented in Sec. III. The discussion in Sec. IV is supported by an appendix, which provides the derivation of burrowing rate as a function of cluster size.

II. EXPERIMENT AND SIMULATION

Co nanoparticles were generated by dc magnetron sputtering (300 W) of a cobalt target (99.95% purity) in a baked ultrahigh vacuum (UHV) chamber (base pressure in the high 10^{-10}-Torr range) backfilled with 1.0 Torr of ultraclean argon (<1 part per billion). This sputter chamber was attached to a UHV-compatible TEM (modified JEOL 200CX,[9] base pressure in the low-10^{-9}-Torr range) via a connecting tube. After sputtering for 30 s in the static argon atmosphere, the argon gas was pumped through the microscope and entrained particles were deposited on the substrate. Further details of the experimental setup, deposition procedure, and substrate preparation have been published elsewhere.[7,10]

This section focuses on the atomistic computer simulations that were performed to gain additional insight into the early stages of the cluster-substrate interaction and to model the strain field caused by a coherent cluster. MD methods[11] were employed to simulate the landing of Co nanoclusters on Cu substrates. Since experiments show that small Co clusters in equilibrium have the fcc rather than the hcp structure expected for bulk Co,[12] the cluster was given the fcc structure. A 10-nm Co cluster was set up in the shape of a Wulff polyhedron with six (001) and eight (111) side facets. In the Wulff construction, which minimizes the surface energy of the cluster, the distance of each facet from the cluster center is proportional to its surface energy. In the case of Co these distances are approximately equal.[13] The cluster was then placed above a Cu(001) surface and directed with low kinetic energy, 0.005 eV/atom, toward the surface. This corresponds roughly to the translational energy of the particles in the experiment. The Cu substrate had more than five times the number of atoms than the Co cluster. Periodic boundary con-

ditions were applied in the *x* and *y* dimensions to mimic an infinite crystal, and the three bottom Cu layers were fixed to prevent unrealistic surface relaxation. Both the Co cluster and Cu substrate were equilibrated for ≈10 ps at constant temperature prior to the impact. The Berendsen temperature control method,[14] with a time constant of 500 fs, was applied to all atoms in the system to keep the temperature at a constant value of 600 K.

Conjugate-gradient (CG) energy minimization[15] with an adaptive step size[16] was used to efficiently calculate the strain field surrounding a Co cluster. Since the TEM observations show that the Co clusters are coherently embedded in Cu (Sec. III), we placed spherical Co clusters at different depths in the Cu matrix, or in bulk Cu. Three atom layers at all cell boundaries, except that at the surface, were fixed to prevent a strain-field contribution from artificial surface relaxations. While this procedure introduces an undesirable truncation of the strain fields, we found by employing cell sizes up to the edge length of 43 nm that size effects did not appreciably alter the strain fields close to the cluster. The strains were determined by comparing the relaxed atom positions with positions in an undistorted Cu matrix.

The embedded-atom method (EAM) interatomic potential from Foiles[17] was employed to describe the interactions in Cu, the EAM potential of Pasianots and Savinos for Co,[18] and our own hybrid potential for the Co-Cu interactions.[19] The Cu and Co potentials are known to give a reasonable description of elastic properties[20] and the Co-Cu potential gives a positive heat of mixing of about the right magnitude for Co-Cu alloys,[19] so that these potentials should adequately describe the present system. The surface energies according to these potentials are 1300 mJ/m^2 for a Cu(001) surface and 1230 mJ/m^2 for an average of low-index Co facets.[21]

III. RESULTS

Co clusters were deposited on a clean Cu(001) surface in the UHV TEM at room temperature. As pointed out in our previous paper,[7] the particles were highly faceted and had a log-normal size distribution with a mean diameter of 13 ± 4 nm. In the selected-area diffraction pattern shown in Fig. 1(a), four Debye-Scherrer rings are visible and coincide with the first four Co fcc rings, proving that the particles are randomly oriented with respect to the substrate. The intensity variation among the rings, however, is unusual, with the (200) ring being much weaker than the (220) ring. To explain this texture, and for further discussion of the particle-substrate orientation, it is important to briefly review the shapes of Co nanoparticles that have been observed in the literature.

The fcc phase is the stable phase for Co particles with diameters[12] up to 110 nm owing to the surface energy of fcc Co that is slightly smaller than that of hcp Co, which is the equilibrium phase in bulk Co.[22] For particles smaller than 10 nm, the stable configuration is a multiply twinned icosahedron with 20 (111) facets. Larger particles appear as a Wulff polyhedron surrounded by eight (111) and six (001) facets. While in early work on nanoparticle formation by inert-gas condensation, only Co nanoparticles in the fcc phase were
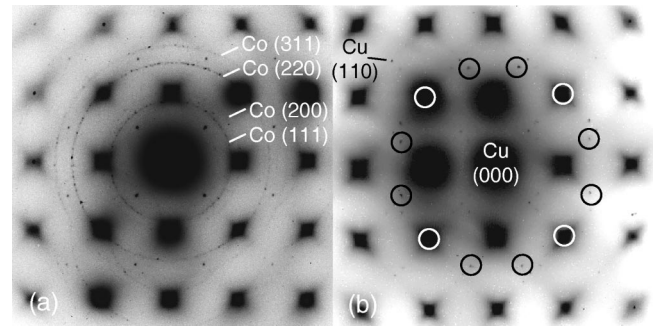
FIG. 1. Selected-area diffraction pattern of Co on Cu(001) at (a) 300 K and (b) 600 K. At 300 K the Co nanoparticles are randomly oriented with respect to the substrate. The first four Co fcc rings are present in the diffraction pattern. At 600 K most particles have assumed the substrate orientation. Their reflections are obscured by the Cu matrix spots. A small fraction of fcc particles is oriented in the $(111)_{Co} \| (001)_{Cu} : \langle 110 \rangle_{Co} \| \langle 110 \rangle_{Cu}$ orientation as discussed in the text. Circles in the diffraction pattern (b) mark the primary reflections resulting from particles in this orientation. The additional spots in (a) and (b) halfway between the Cu reflections are a feature of the Cu foil (Ref. 38).

observed,[23,24] more recent work has shown that metastable hcp particles are also produced by magnetron sputtering, depending on the exact sputtering conditions.[12,25,26] hcp Co particles are Wulff polyhedrons with (001) and (011) facets.[12] We also observed both fcc and hcp phases: Deposition of the particles under identical conditions on an amorphous carbon film gave rise to both fcc and hcp rings in the diffraction pattern.

In the diffraction pattern of Fig. 1(a), however, only fcc rings are visible and, moreover, the (200) ring is fairly weak. This indicates that most particles are in a ⟨111⟩ zone axis configuration and, since the ⟨111⟩ direction is not orthogonal to ⟨200⟩, they do not give rise to a (200) reflection (Weiss zone law). On the crystalline substrate the particles preferentially land on one of their facets. Assuming the majority of the particles consists of multiple twinned icosahedrons and hcp Co particles, the ⟨111⟩ texture in the diffraction pattern can be explained. Multiple twinned icosahedrons only have (111) facets and therefore do not give rise to a (200) reflection. hcp Co particles give rise to (100) and (101) rings with their (001) and (011) facets and these are sufficiently close to the fcc (111) and (220) rings to be unresolved in Fig. 1(a). fcc Co particles have both (111) and (001) facets. If the surface energies of these two faces are equal, as assumed in Sec. II, both types of facets cover approximately the same solid angle.[27] 50% of the fcc Co particles thus contribute to the intensity in the (200) ring. Note that this fraction is very sensitive to the ratio of surface energies. In a Wulff cluster where the surface energy of a (111) face amounts to 87% of the (001) surface energy, the (001) faces cover only 20% of the entire solid angle.

The particles were then deposited on a substrate held at 600 K. In the diffraction pattern in Fig. 1(b) the Co Debye-Scherrer rings have disappeared, and the vast majority of the Co particles has assumed the (001) orientation of the Cu substrate. A small fraction of the particles has assumed a
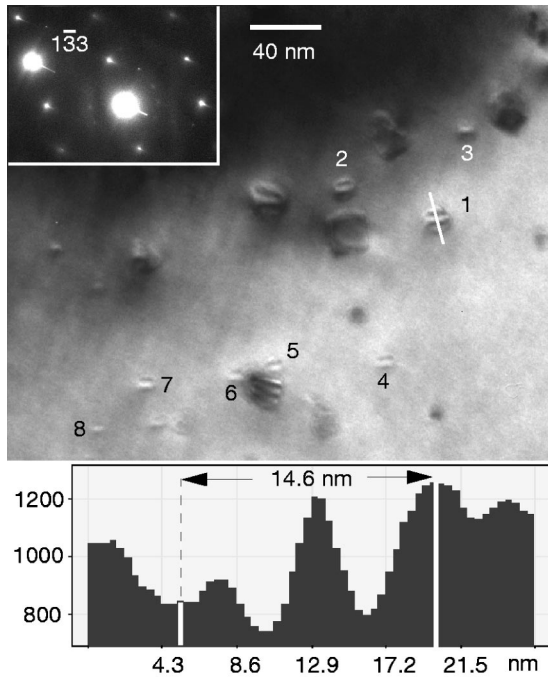
FIG. 2. $(1\bar{3}3)$ dark-field micrograph of Co on Cu(001) taken under exact two beam conditions. The insert at the top left corner shows the selected-area diffraction pattern. An intensity profile along the white line through particle 1 is displayed at the bottom. In this case, twice the distance r_x between the particle center and the third extremum is 14.6 nm.

different orientation and gives rise to faint extra spots in Fig. 1(b). These spots arise from fcc particles in a different orientation. Their (111) planes are parallel to the Cu(001) surface and their $\langle 110 \rangle$ direction is aligned with the Cu$\langle 110 \rangle$ direction. Each particle only gives rise to six spots, but since there are two independent $\langle 110 \rangle$ orientations on the Cu(001) surface, a large number of clusters lying on equivalent orientations gives rise to the 12 spots, which are marked in Fig. 1(b). All other spots visible are the result of double diffraction. A similar orientational relationship was observed for Ag particles on Cu(001).[5] While a hcp particle landing with a (001) facet parallel to the Cu surface could cause an identical spot pattern, a (011) facet would give rise to additional spots that are not present in Fig. 1(b).[28] This implies that the hcp particles have transformed into the equilibrium fcc structure at 600 K, and is in agreement with other observations.[12]

Due to a 2% difference in lattice constant, the particles in the $(001)_{Co} \| (001)_{Cu}$ orientation coherently strain the matrix. The resulting image contrast, shown in Fig. 2, is very similar to that reported by Ashby and Brown[29] for coherent Co precipitates inside a Cu matrix. They simulated the image contrast by numerically integrating the two-beam Howie-Whelan equations, which was possible since in the bulk case the strain field of a coherent inclusion has an analytical solution. For inclusions close to a surface, however, this method cannot be applied. Recently, Miller, Liu, and Gibson[30] developed a method to accurately measure the average strain in an individual particle close to a surface. We employ this technique and then deduce the depth of the par-

ticles by comparison with strain values obtained by computer simulations of a Co particle in a Cu matrix at various depths.

Miller, Liu, and Gibson show that most features of strain contrast can be simulated adequately using a simplified strain model, called the abrupt displacement approximation (ADA). The strain field is assumed to be parametrized in cylindrical coordinates with the z direction normal to the substrate. The main assumptions of the ADA are that the strain field extends only a small distance into the sample in the z direction, compared with the electron extinction distance and that the radial component of the displacements depends linearly on the radius. Beyond the edge of the particle the only requirement is that the strain field decays sufficiently fast. The continuously varying displacement field can then be replaced by a step function, assumed to be cylindrically symmetric, at a fixed depth z_0 a short distance into the substrate. The size of the step increases linearly from the center to the edge of the particle.[31] In the framework of this model, which reportedly works well for Si-Ge quantum dots,[32] qualitative features of the image contrast can be obtained. The average radial strain ε can be determined by simply taking an intensity profile across an individual particle parallel to the diffraction vector **g**. The average distance r_x between the particle center and equivalent extrema on either side of the particle is measured and ε is obtained from the equation

$$(2n-1)\frac{\pi}{2} = 2\pi|\mathbf{g}|\varepsilon r_x, \qquad (1)$$

where n is the order of the extremum considered. Measurements must be performed under exact two-beam conditions with a high-order reflection **g**. Since it was not possible to tilt the specimen inside the UHV TEM, our measurements were carried out *ex situ* in a Philips CM12 TEM. For the $(1\bar{3}3)$ dark field image shown in Fig. 2 the sample had been tilted to a $\langle 310 \rangle$ zone axis. The intensity profile across one particle is shown at the bottom of Fig. 2 for illustration. The accuracy of this method is limited by how well the position of the fringes in the particles can be determined. The strain values obtained are thus accurate to $\approx 10\%$. The average strain for the labeled particles in Fig. 2 is 1.5%.

By using conjugate-gradient (CG) simulations, we calculated the radial displacements for a 5-nm Co cluster embedded coherently in Cu as a function of the cluster depth. The displacement field was then parametrized in cylindrical coordinates as shown in Fig. 3(a) for a half-buried cluster. It demonstrates that the displacements decay rapidly with depth compared to the extinction distance of 75 nm for a $(1\bar{3}3)$ reflection in Cu.[33] In Fig. 3(b) the three-dimensional plot of Fig. 3(a) has been projected into the displacement-radius plane. The maximum displacements rise linearly as a function of radius up to the edge of the particle and then decay proportionally to $r^{-2.7}$. The assumptions of the ADA are therefore satisfied in this system. The radial strain, i.e., the average of the relative radial Co displacements, determined from the simulation of a 5-nm cluster at various positions relative to the surface, is plotted as a function of the cluster
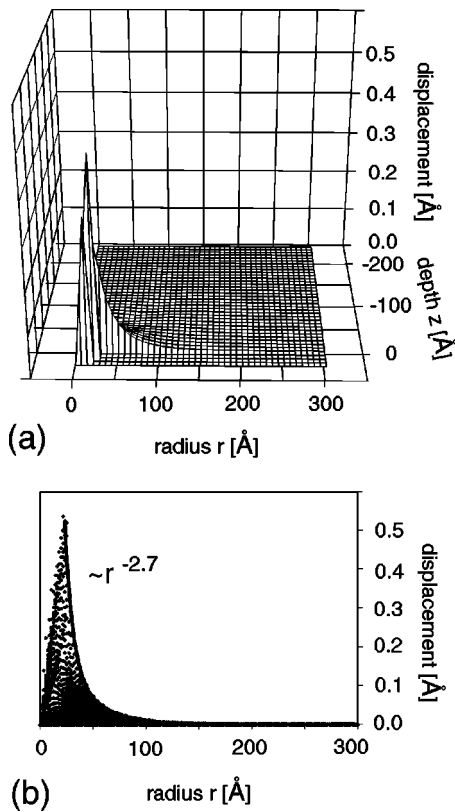
FIG. 3. Computer modeling of the Cu displacement field for a 5-nm Co cluster half buried in the Cu matrix. In (a) the radial displacements in cylindrical coordinates are plotted (averaged over φ), and (b) shows a projection into the radius-displacement plane, together with a fitted curve for the maximum displacement outside the particle.

depth in Fig. 4. The curve asymptotically reaches a strain of 1.6%, which compares well with a value of 1.58% derived from elasticity theory.[34] Furthermore, since the strain of a coherent inclusion in an infinite isotropic matrix depends, to first order, only linearly on the misfit of the two materials, and since the misfit is one fitting parameter of the EAM potentials, the simulated strain values should be accurate to within 5%.
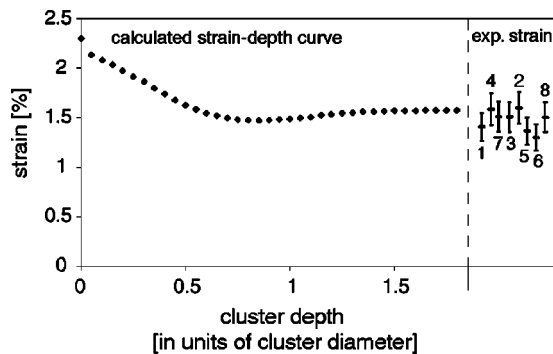
FIG. 4. Calculated (for a 5-nm cluster) dependence of the strain on the depth of the cluster, expressed in fractions of its diameter. The measured strain values from Fig. 2 are also plotted in this graph. Note that the strain is defined as the displacement of Co atoms relative to the undisturbed Cu lattice positions.
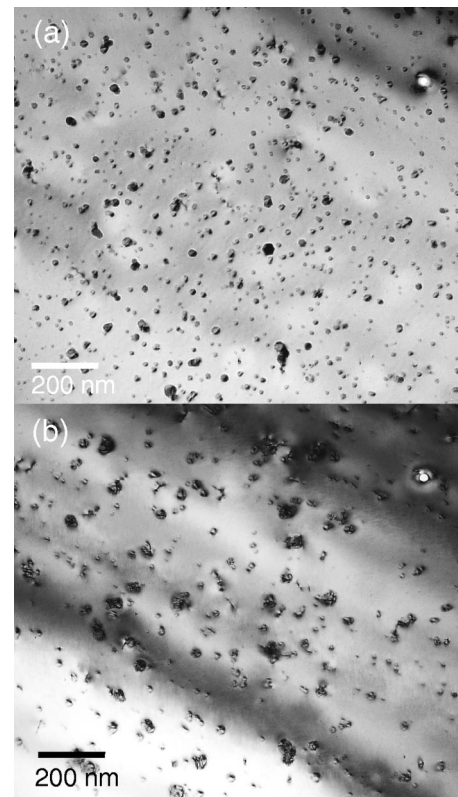
FIG. 5. (a) Bright-field micrograph of Co deposited on Cu(001) at 600 K. Upon annealing at 750 K the particles agglomerate. The bright field taken after the annealing treatment (b) shows exactly the same area as (a).

The strain-depth curve of Fig. 4 shows a considerable dependence on depth for the initial stages of burrowing. For clusters buried almost completely beneath the surface, the strain reaches its minimum value. The measured strain values from Fig. 2, which are included in Fig. 4, fall predominantly in the vicinity of this minimum. They are incompatible with particles on the surface and thus provide convincing evidence, merely from plan-view TEM, of burrowing for deposition at 600 K. These measurements are further complemented by atomic force microscope (AFM) scans published previously.[7]

Upon annealing the sample that was deposited at 600 K at 750 K, the particles began to agglomerate, as shown, for example, in Fig. 5, with the larger particles growing at the expense of smaller particles. The distribution of the particles by number is trimodal at 750 K, with the original peak at 13 nm and additional peaks at 27 ± 2 and 41 ± 7 nm. Only 25% of the initially deposited particles retain their average size of 13 nm. The particles do not change their orientation relative to the substrate, but the contrast of those particles with an average size of 41 nm indicates the presence of dislocations and thus semicoherent interfaces. The lack of time-dependent data precludes further quantification of this ripening behavior, but the following scenario seems likely. First, Co in buried particles contingent with the surface diffuses across the surface to other buried particles, allowing them to grow preferentially in the surface region. This eventually leads to
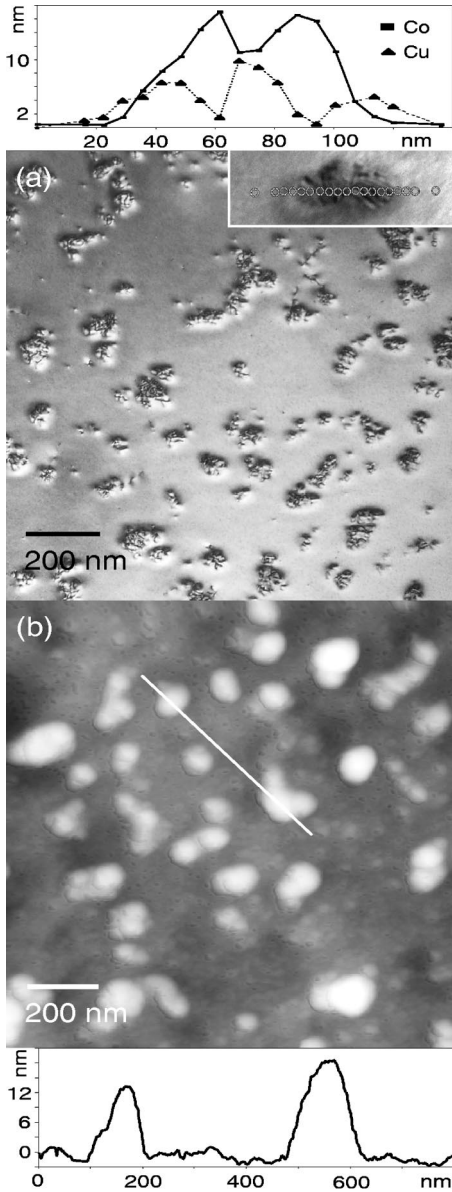
FIG. 6. (a) Bright-field and (b) AFM characterization (different areas) of a sample annealed to 900 K. The top graph shows the thickness of a typical island as determined from the Co EDX signal. The EDX counts far from the island were used as thickness calibration. Also shown is the amount of additional Cu around the particle. The EDX measurements have been performed on the spots marked on the enlarged particle. The AFM height profile through two particles along the white line is illustrated at the bottom of this figure. Note that the size of the particles is similar to the one shown in the EDX scan.

platelike particles on the surface, coated with Cu. Such situations were observed as shown in Fig. 6. Here a sample with high coverage at 600 K had been annealed to 900 K. Most of the particles have completely disappeared from the matrix while a few large islands have formed [Fig. 6(a)]. The white halo around the particles indicates some residual strain. By performing energy dispersive x-ray analysis (EDX) measurements along a line through a particle and using the bare Cu film as calibration, the particle thickness could be estimated.

The insert in Fig. 6(a) shows a typical scan through an island. Plotted are the Co height profile and the amount of Cu in excess of the average film thickness. A Cu coating of the particle is clearly visible. By repeating the EDX measurements for different sample tilt angles we verified that changing x-ray intensities due to changing diffraction conditions across the island did not affect the measurements. The surface features in the corresponding AFM scans, shown in Fig. 6(b), are of similar height, which implies that the particles are indeed located on the surface. We show in Sec. IV that this configuration is energetically more favorable than the bulk location owing to the increasing strain energy of an inclusion with size. While the strain energy is negligible for 13-nm particles, a residual strain of ≈0.5% is sufficient to stabilize the larger particles on the surface. Upon further annealing at 1150 K the particles eventually dissolved into the Cu matrix, since bulk diffusion becomes appreciable and there is ≈2% solubility of Co in Cu at this temperature.[35]

IV. DISCUSSION

The basic driving force for the sinking process, which we also observed for Co nanoparticles on Ag(001),[7] is the reduction in total free energy by exchanging the Co-vacuum interface above the surface with a Co-substrate interface below the surface without increasing the substrate surface area or, significantly, the elastic strain. This process, as it was shown previously,[7] is likely to occur in two steps: first, coating of the particle with substrate material, and second, burrowing. In both steps, the total free energy of the system is reduced. The capillary forces associated with this reduction in surface area drive the particle inward.[7] Neglecting strain effects, the time dependence of burrowing can be approximated by the following equation:

$$t = \alpha \frac{kT}{V_m \gamma \delta D} r^4, \qquad (2)$$

where α is a geometric factor, which has a value of ≈1.1 in our model. V_m is the volume of one substrate atom, γ is the substrate surface energy, D denotes the diffusion coefficient along the cluster substrate interface of width δ, r is the cluster radius, and kT has its usual meaning. Details can be found in the Appendix to this work. For Co clusters on Ag(001) Eq. (2) yields burrowing times that agree well with the time scales in the experiment.[7]

The situation for Co clusters on Cu(001) is complicated by the coherent interface and the associated strain field. We point out first that the energetics of the system are not much affected by strain, at least for nanoparticles. The strain energy E_{sb} of a spherical cluster embedded coherently in the bulk is[36]

$$E_{sb} = \frac{2\mu_m K_i}{3K_i + 4\mu_m} \left(\frac{\Delta V}{V}\right)^2 V, \qquad (3)$$

where μ_m is the shear modulus of the lattice, K_i the bulk modulus of the inclusion, ΔV the volume change of the cluster upon inclusion in the matrix, and V the original volume of the cluster. Our simulations, described in Sec. II, verify that Eq. (3) describes to good approximation the strain energy of a partially embedded cluster. V in this case represents

the volume of only that part of the cluster that is embedded in the film, while the ratio $\Delta V/V$ remains unchanged. For the Co-Cu system, Eq. (3) yields $E_{sb}=8\times10^7$ J/m^3 times the cluster volume. The strain energy can therefore be reasonably neglected for Co particles ≈ 10 nm in diameter in its contribution to the total free energy of the system. With growing particle size, however, the strain energy eventually becomes dominant due its volume dependence and can stabilize larger clusters on the surface, as mentioned in Sec. III. Equation (2) again yields burrowing times in agreement with the experiment.[7]

To help elucidate the reorientation behavior of the clusters that was observed in Sec. III we used MD simulations of faceted, 10-nm-diam Co particles landing on Cu(001) at 600 K. The Co clusters were set up in the equilibrium fcc phase, in order to avoid having to simulate the hcp to fcc phase transition that was observed in hcp particles in Sec. III. For Co particles landing on a (001) facet (with the facet normal being within about 10° of the substrate normal) the alignment became perfect within some 50 ps. This shows that perfect epitaxy can be achieved very quickly, at least when the cluster facet hits the surface close to matching surface directions. On the other hand, Co particles landing with a (111) surface nearly parallel to the Cu(001) surface rocked back and forth on the surface several times during the first 200 ps following impact. Note that for a 10-nm cluster the initial translational kinetic energy was about 200 eV, which is larger than the energy associated with cluster-substrate bonds across the interface. For smaller cluster sizes this condition no longer holds, and then rocking was not observed. Following this rocking motion, the cluster rotated some 10° over the next 100 ps, before settling in a fixed position during the last 300 ps of the simulation. The final orientation was $(111)_{Co}\|(001)_{Cu}$ with the $\langle110\rangle$ directions of each plane aligned (see Fig. 7), which was experimentally observed for a small number of particles in the diffraction pattern of Fig. 1(b).

Based on these results and the time scales involved, the following scenario for reorientation seems likely: fcc particles, which land on the surface with a (111) or (001) facet, assume the metastable $(111)_{Co}\|(001)_{Cu}:\langle110\rangle_{Co}\|\langle110\rangle_{Cu}$ orientation or the $(001)_{Co}\|(001)_{Cu}:\langle100\rangle_{Co}\|\langle100\rangle_{Cu}$ orientation, respectively. This occurs on a time scale of nanoseconds at 600 K. They then burrow into the substrate as outlined earlier, and all particles reorient in the $(001)_{Co}\|(001)_{Cu}$ configuration during this time. In hcp particles the burrowing and reorientation is accompanied by a transformation into the fcc phase. The small fraction of particles remaining in the $(111)_{Co}\|(001)_{Cu}:\langle110\rangle_{Co}\|\langle110\rangle_{Cu}$ orientation may in fact be those that did not burrow.

An important result of this work is the demonstration that the strain field around the Co cluster in Cu can be measured accurately by TEM. This has been used here in a novel way to obtain the depth of the particles in plan-view TEM. The accuracy of the theoretical strain depth curve, which was obtained with the help of MD simulations, has already been pointed out in Sec. III. It allows us to draw another conclusion here. The strain values measured in Fig. 2 are plotted as a function of particle size in Fig. 8. The slight decrease of the
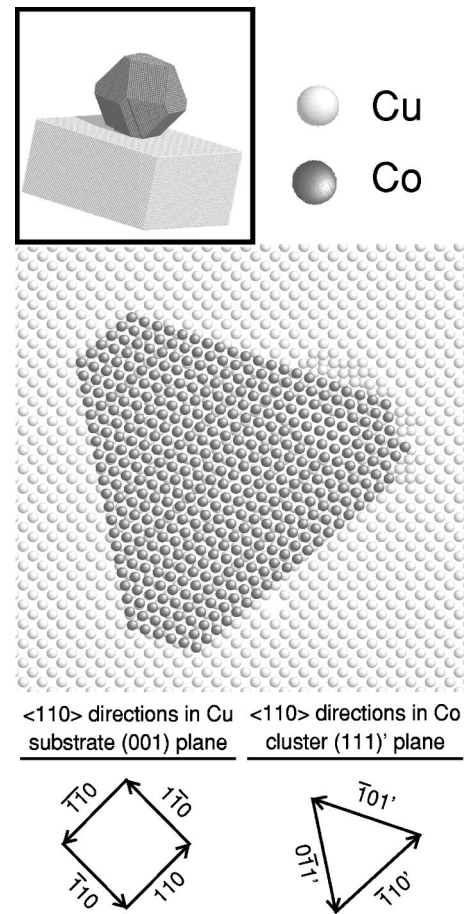
FIG. 7. Orientation of a 10-nm Co cluster with the Cu substrate. The darker spheres are Co atoms and the lighter ones Cu atoms. The Co cluster initially hits the surface with a (111) lattice plane almost parallel to the (001) Cu surface, and subsequently rotates to find a reasonable lattice match. The simulation was carried out at 600 K, but to plot the figure the cell was quenched down to 0 K to remove thermal vibrations. The insert in the top right-hand corner shows the positions of all atoms 600 ps after impact. The quadratic cluster side facets are (001) planes and the hexagonal facets (111) atom planes. Note the atom step edge on the top and front lower side (111) facets: although the cluster was initially perfect, during the initial impact (at about 40 ps) part of the cluster slipped by $\frac{1}{6}$ of a nearest-neighbor distance in a $\langle112\rangle$ crystal direction on a (111) side plane, i.e., along the slip system of fcc metals. The positions of atoms on one atom plane on both sides of the Co/Cu interface at 600 ps are shown enlarged. The $\langle110\rangle$ crystal directions on the Cu(001) surface and the Co bottom (111)′ layer are illustrated. Since the cluster and substrate are not coherent and hence have different lattice vector systems, a prime is used to denote the Co lattice vectors. The $\langle\bar{1}10'\rangle$ lattice vector in Co has aligned almost perfectly with the $\langle110\rangle$ vector in the Cu substrate.

measured strain with particle size can be reproduced well in the calculations by assuming all particles are buried right underneath the surface. In addition, the average strain values are below the 1.6% expected for particles well inside the Cu matrix. This serves as additional evidence, next to the cross-sectional TEM analysis published previously,[7] that the particles burrow until they are completely embedded in the film,
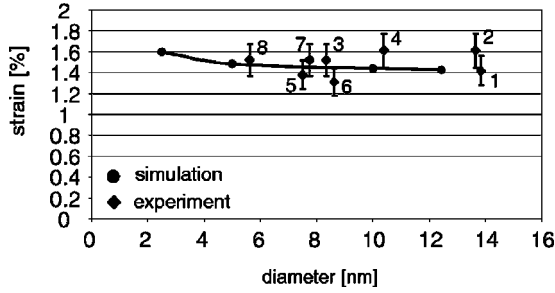
FIG. 8. The strain measured in each labeled particle in Fig. 2, according to the abrupt displacement approximation, is plotted against the particle diameter. Also included are the calculated strain values, assuming the clusters are buried just below the surface.

but not further. This is in agreement with the detailed analysis of the time dependence of this process outlined in the Appendix. The burrowing time diverges logarithmically once the cluster is buried (almost) completely.

V. CONCLUSIONS

We have investigated the smoothing behavior of heterogeneous surfaces prepared with nonequilibrium roughness by depositing Co nanoparticles on Cu(001) surfaces. For this system we found a new kinetic pathway for surface smoothing, which we term burrowing, that allows single particles to reach their equilibrium configuration beneath the surface. Burrowing is driven by the extremely large capillary forces associated with nanoparticles. Since it requires only diffusion along the particle substrate interface and not bulk diffusion, we observed it at temperatures as low as 600 K. This work suggests that burrowing should occur in all systems where the nanoparticles have a significantly higher surface energy than the substrate. Particles with smaller surface energy would simply wet the substrate. We have shown, moreover, that the time for particles to burrow varies as r^4, which implies that this smoothing mechanism is kinetically forbidden in micron-and larger-sized systems.

We have further demonstrated that on Cu(001) the Co particles assume epitaxial relationships with the substrate. The strain associated with a coherent interface gives rise to additional features in this particular system. A new method, the abrupt displacement approximation, made quantification of the strain in individual particles possible. The strain also affects the energetics of the system. Once larger particles have formed on the surface, for example, by further annealing of the sample, they are stabilized against burrowing by the strain energy.

MD simulations were employed to obtain the strain depth dependence of an embedded particle close to the surface, thus enabling us to obtain depth information on the particles. Very good agreement with the values calculated from elasticity theory was obtained for particles in bulk samples. Finally additional insight concerning the initial stages of cluster reorientation was gained with the help of the simulation.

ACKNOWLEDGMENTS

APPENDIX

This estimate of the time required for burrowing follows closely the procedure of Chu *et al.*[37] We make the assumption that the cluster remains spherical throughout the burrowing process and that the Cu coating assumes the particle shape, i.e., plastic deformation and neck formation are ignored (they would not be the rate-determining steps in any case). The calculations can be conveniently divided into three steps: (i) First, the capillary force, which is the driving force for this burrowing process, is derived from the change in surface area while the cluster is sinking. (ii) This force drives the diffusion of material from underneath the spherical cluster along the cluster-substrate interface. Conservation of mass leads to an expression for the flux along this interface. The flux can then be related to the chemical potential around the cluster and ultimately to a force balancing the capillary force derived in step (i). (iii) In the last part we finally derive the burrowing time.

Calculation of the capillary force on the particle

The change in the total free energy $E(z)$ of the system as a function of the cluster depth z [measured from the bottom of the cluster relative to the surface; see Fig. 9] is calculated. We assume that the cluster is coated with substrate atoms (surface tension γ) and that the displaced material diffuses away and forms an additional surface layer, i.e., that it can be neglected here. $E(z)/\gamma$ is made up out of three parts: the surface of the sphere not buried yet, the original surface area of the substrate and the reduction in substrate surface area

$$E(z) = \gamma\{2\pi R(2R-z) + \pi R^2 - \pi[R^2 - (R-z)^2]\}. \tag{A1}$$

Taking the negative derivative of $E(z)$ the force on the cluster is obtained:

$$F(z) = -2\pi\gamma(z-2R). \tag{A2}$$

This force on the cluster drives the diffusion and results in its movement with a velocity v.

Calculation of the diffusion along the cluster substrate interface

Figure 9 shows the geometry considered in the flux calculations. Spherical coordinates are used, and due to the symmetry of the problem the flux along the interface of width δ has only a component parallel to the cluster surface and depends only on θ [$j_\theta(\theta)$]. The assumption made here is that the cluster radius R is much larger than δ; in other words, there is no radial flux dependence. While the cluster
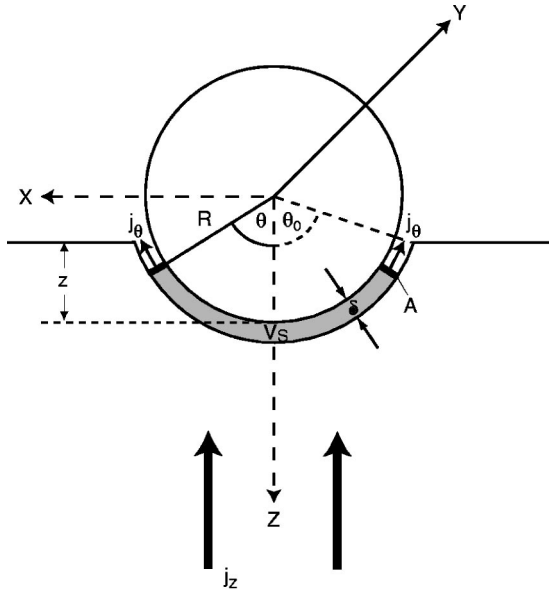
FIG. 9. Geometry used in the derivation of the burrowing time.

is sinking, there is an incoming flux of substrate atoms into the interface area (in Fig. 9 the interface area under consideration extends up to θ_0; an arbitrary part V_s of it is shaded). Note that we treat this problem in a coordinate system that is fixed in the particle; therefore the grain boundary does not move. If the cluster is sinking with a velocity v, this flux j_z in the z direction is given by

$$j_z = v \frac{1}{V_m}, \qquad (A3)$$

where V_m is the volume of one substrate atom. Furthermore we assume that the diffusion along this interface is always in a steady state, i.e., there are no changes in concentration with time. The conservation of mass then yields

$$\operatorname{div}\mathbf{j}=0 \Leftrightarrow \int_{V_s} \mathbf{j}\, d\mathbf{A}=0. \qquad (A4)$$

Evaluating this with the fluxes defined above results in

$$0 = A j_\theta - \int_0^\theta \int_0^{2\pi} j_z \mathbf{e}_z \cdot \mathbf{e}_r R^2 \sin\theta\, d\theta\, d\varphi. \qquad (A5)$$

The product between $\mathbf{e}_z$ and $\mathbf{e}_r$ contributes $\cos\theta$. Area A (compare Fig. 9) is part of a cone surface and equals $2\pi R \delta \sin\theta$ when neglecting terms of the order δ^2. By combining Eqs. (A3) and (A5), j_θ is derived:

$$j_\theta = v \frac{1}{2\delta V_m} R \sin\theta. \qquad (A6)$$

The next step is to relate j_θ to the chemical potential μ along the interface via the diffusion equation

$$\mathbf{j}=-K\boldsymbol{\nabla}\mu, \qquad K=\frac{D}{kT}\frac{1}{V_m}. \qquad (A7)$$

D is the diffusion coefficient, k the Boltzmann constant, and T the temperature. Equations (A6) and (A7) result in

$$\mu(\theta)=\frac{v}{K}\frac{1}{2\,\delta V_m}R^2\cos\theta+C, \qquad (A8)$$

where C is an integration constant. We neglect shearing stresses, as they cannot affect the magnitude of the normal stresses, and the (hydrostatic) pressure p around the cluster is estimated by

$$\mu(\theta)=p(\theta)V_m, \qquad (A9)$$

with $p(\pi/2)=0$, i.e., C has to be chosen as 0. The total force on the cluster at this depth can be calculated by integrating the normal component of $p(\theta)d\Omega$ up to θ_0 ($d\Omega$ is a unit element of surface area on the sphere, i.e., $R^2\sin\theta\, d\theta\, d\varphi$):

$$F(z)=\int_0^{\theta_0}\int_0^{2\pi} p(\theta)\cos\theta\, d\Omega. \qquad (A10)$$

The relation between the depth z and θ_0 can be derived straightforwardly and Eqs. (A8)–(A10) yield

$$F(z)=v\frac{\pi kT}{3V_m\delta D}R[R^3-(R-z)^3]. \qquad (A11)$$

Derivation of the time required for burrowing

Combining Eqs. (A2) and (A11) and taking into account that v equals dz/dt, one obtains

$$\frac{dz}{dt}=\frac{6V_m\delta D}{kT}\frac{\gamma}{R}\frac{2R-z}{R^3-(R-z)^3}, \qquad z\in[0,2R]. \quad (A12)$$

This equation can be integrated to

$$t(z)=\frac{1}{6}\frac{kT}{V_m\delta D\,\gamma}R\left\{2R^3\ln\frac{2R}{2R-z}-R^2z+R\frac{z^2}{2}-\frac{z^3}{3}\right\}. \qquad (A13)$$

Therefore the time it takes for the cluster to become buried up to $z=0.99(2R)$ is

$$t(z)=1.1\frac{kT}{V_m\delta D\,\gamma}R^4. \qquad (A14)$$

---

*Present address: Accelerator Laboratory, P.O. Box 43, FIN-00014 University of Helsinki, Finland.

†Present address: Department of Materials Science, National University of Singapore, Singapore 119260.

‡Present address: Materials Science Division, Argonne National Laboratory, 9700 South Cass Avenue, Argonne, IL 60439-4838.

§Present address: Materials Division, Faculty of Engineering, Ulm University, 89081 Ulm, Germany.

‖Present address: I. Physikalisches Institut, Universität Göttingen, 37073 Göttingen, Germany.

[1] C. Herring, in *The Physics of Powder Metallurgy*, edited by E. Kingston (McGraw-Hill, New York, 1951), 143.

[2] W. W. Mullins, J. Appl. Phys. **30**, 77 (1959).

[3] M. E. Keeffe, C. C. Umbach, and J. M. Blakely, J. Phys. Chem. Solids **55**, 965 (1994).

[4] F. A. Nichols and W. W. Mullins, J. Appl. Phys. **36**, 1826 (1965).

[5] M. Yeadon, M. Ghaly, J. C. Yang, R. S. Averback, and J. M. Gibson, Appl. Phys. Lett. **73**, 3208 (1998).

[6] M. Yeadon, J. C. Yang, R. S. Averback, J. W. Bullard, D. L. Olynick, and J. M. Gibson, Appl. Phys. Lett. **71**, 1631 (1997).

[7] C. G. Zimmermann, M. Yeadon, K. Nordlund, J. M. Gibson, R. S. Averback, U. Herr, and K. Samwer, Phys. Rev. Lett. **83**, 1163 (1999).

[8] In a recent paper [S. Padovani, F. Scheurer, and J. B. Bucher, Europhys. Lett. **45**, 327 (1999)] burrowing of Co dusters, containing less than 200 atoms, into Au(111) surfaces was observed. We believe, however, that a different burrowing mechanism is operative in this size regime.

[9] M. L. McDonald, J. M. Gibson, and F. C. Unterwald, Rev. Sci. Instrum. **60**, 700 (1989).

[10] D. L. Olynick, J. M. Gibson, and R. S. Averback, Mater. Sci. Eng., A **204**, 54 (1995).

[11] M. P. Allen and D. J. Tildesley, in *Computer Simulation of Liquids* (Oxford University Press, Oxford, 1989).

[12] O. Kitakami, H. Sato, Y. Shimada, F. Sato, and M. Tanaka, Phys. Rev. B **56**, 13 849 (1997).

[13] M. Aldén, S. Mirbt, H. L. Skriver, N. M. Rosengaard, and B. Johanson, Phys. Rev. B **46**, 6303 (1992).

[14] H. J. C. Berendsen, J. P. M. Postma, W. F. van Gunsteren, A. DiNola, and J. R. Haak, J. Chem. Phys. **61**, 3684 (1984).

[15] W. H. Press, S. A. Teukolsky, W. T. Vetterling, and B. P. Flannery, in *Numerical Recipes in C: The Art of Scientific Computing* (Cambridge University Press, New York, 1995).

[16] K. Nordlund, P. Partyka, R. S. Averback, I.K. Robinson, and P. Ehrhart, J. Appl. Phys. **88**, 2278 (2000).

[17] S. M. Foiles, Phys. Rev. B **32**, 3409 (1985).

[18] R. Pasianot and E. J. Savino, Phys. Rev. B **45**, 12 704 (1992).

[19] K. Nordlund and R. S. Averback, Phys. Rev. B **59**, 20 (1999).

[20] M. S. Daw, M. Foiles, and M. I. Baskes, Mater. Sci. Rep. **9**, 251 (1993).

[21] In all energy calculations the experimental surface energy values of 1800 m/m^2 for Cu and 2190 m/m^2 for Co [W. R. Tyson and W. A. Miller, Surf. Sci. **62**, 267 (1977)] were used. In the cases where the strain energy was calculated by simulation, the interface and surface energy contributions of the interatomic potential were removed to obtain the strain energy only. Since the interatomic potentials reproduce the elastic constants well, this quantity is reliably given by the simulation.

[22] M. Hansen, *Constitution of Binary Alloys* (McGraw-Hill, New York, 1958).

[23] K. Kimoto, Y. Kamiya, M. Nonoyama, and R. Uyeda, Jpn. J. Appl. Phys., Part 1 **2**, 702 (1963).

[24] A. R. Thölen, Acta Metall. **27**, 1765 (1979).

[25] E. Anno, Phys. Rev. B **50**, 17 502 (1994).

[26] H. Sato, O. Kitakami, T. Sakurai, Y. Shimada, Y. Otani, and K. Fukamichi, J. Appl. Phys. **81**, 1858 (1997).

[27] This follows directly from the Wulff construction. The solid angles were calculated from the Wulff cluster which was set up in the MD simulations in Sec. III.

[28] The direction normal to a hcp (011) facet is $\langle 1\,2\,0.57\rangle$. A particle landing with its (011) facet on the Cu surface is therefore in between a $\langle 241\rangle$ and a $\langle 362\rangle$ zone axis configuration. The resulting diffraction pattern gives rise (for any rotation of the particle) to a spot pattern different from the Cu(001) or the $(111)_{Co}\|(001)_{Cu}:\langle 110\rangle_{Co}\|\langle 110\rangle_{Cu}$ pattern.

[29] M. F. Ashby and L. M. Brown, Philos. Mag. **8**, 1083 (1963).

[30] P. D. Miller, C. P. Liu, and J. M. Gibson, Ultramicroscopy **84**, 225 (2000).

[31] Compare Fig. 2 in Ref. 32.

[32] P. D. Miller, C. P. Liu, W. L. Henstrom, J. M. Gibson, Y. Huang, P. Zhang, T. I. Kamins, D. P. Basile, and R. S. Williams, Appl. Phys. Lett. **75**, 46 (1999).

[33] P. Hirsch, A. Howie, R. Nicholson, D. W. Pashley, and M. J. Whelan, *Electron Microscopy of Thin Crystals* (Krieger, Malabar, Florida, 1977), p. 510.

[34] According to N. F. Mott and F. R. N. Nabarro, Proc. Phys. Soc. London **52**, 86 (1940); with material data taken from C. Kittel, *Introduction to Solid State Physics*, 4th ed. (Wiley, New York, 1971), p. 143; G. W. C. Kaye and T. H. Laby, *Tables of Physical and Chemical Constants*, 14th ed. (Longman, London, 1973), p. 31.

[35] *Binary Alloy Phase Diagrams*, 2nd ed., edited by T. Massalski, H. Okamoto, P. R. Subramanian, and L. Kacprzak (ASM International, Materials Park, Ohio, 1990), p. 1181.

[36] J. D. Eshelby, in *Solid States Physics*, edited by F. Seitz and D. Tumbull (Academic, New York, 1956), Vol. 3, p. 79.

[37] M. Y. Chu, M. N. Rahaman, L. C. De Jonghe, and R. J. Brooket, J. Am. Ceram. Soc. **74**, 1217 (1991).

[38] D. Cherns, Philos. Mag. **30**, 549 (1974).